J. Phys. B: At. Mol. Opt. Phys. **32** (1999) 825–835. Printed in the UK PII: S0953-4075(99)96199-0

Total and differential cross sections for medium-energy $H^+ + C_2H_2$ collisions

S Cheng and Y Liu

Department of Physics and Astronomy, The University of Toledo, Toledo, OH 43606, USA

Received 25 July 1998, in final form 6 November 1998

Abstract. Total and/or differential cross sections for single electron capture, single ionization, double ionization, and electron capture plus ionization have been measured for collisions of protons at energies of 6, 12.5, 25, and 50 keV with C_2H_2 molecules. Two-dimensional position-sensitive detectors were used for both the projectile and recoil particle detection. Coincidences between the recoil time-of-flights and the projectile charge states were used to distinguish different collision processes to obtain the total cross sections for those processes listed above. The total and differential cross sections for each process were put on an absolute scale by a normalization to a known collision process.

1. Introduction

Studies of total and differential cross sections for low-energy ions colliding with molecules attract varied interest. They provide fundamental information for atomic and molecular spectroscopy dynamics and the interaction potentials between the colliding particles to assess the validity of proposed models. They also provide data required for modelling the behaviour of physical processes in plasmas and planetary atmospheres. In particular, astrophysicists feel that a systematic study is urgently needed of molecular formation and fragmentation as a result of proton interaction with C_nH_m clusters, which are abundant in astrophysical environments, in order to understand the evolution of our galaxy and even the origin of life on Earth [1, 2]. At present, the few experimental and theoretical studies for low-energy and thermal energy ion impact have concentrated on methane molecules ([3] and references therein) and photoionization experiments with acetylene molecules [4–9]. It is our intention to carry out a series of experimental work for low- and medium-energy proton impact on C_nH_m molecules to measure the total and differential cross sections using our newly built atomic collision beam line and data acquisition system. The first system studied in this series, the C_2H_2, is reported in this paper.

In this paper we report a study of collisions of H^+ at energies of 6, 12.5, 25 and 50 keV with C_2H_2 and provide the first experimental results for the total and differential cross sections for the collision processes listed below. Coincidences between the recoil time-of-flights (TOFs) and the projectile charge states were used to separate different recoil channels involved in these processes.

Energy transfers in collisions of H^+ with C_2H_2 lead to various scattering processes such as excitation and ionization of the C_2H_2 molecules, and electron capture by the projectile H^+ from the C_2H_2 with or without additional ionization of the C_2H_2 molecules. Among those products, excited states such as $C_2H_2^*$ and $(C_2H_2^+)^*$ may also be involved. In this experiment,

0953-4075/99/030825+11$19.50

we concentrate on the following collision processes and the cross sections associated with these processes:

(a) Single ionization (SI) process with cross section σ_{SI}:

$$H^+ + C_2H_2 \rightarrow H^+ + C_2H_2^+ + e$$

(b) Double ionization (DI) process with cross section σ_{DI}:

$$H^+ + C_2H_2 \rightarrow H^+ + C_2H_2^{2+} + 2e$$

(c) Single capture (SC) process with cross section σ_{SC}:

$$H^+ + C_2H_2 \rightarrow H + C_2H_2^+$$

(d) Capture with additional ionization (TI) process with cross section σ_{TI}:

$$H^+ + C_2H_2 \rightarrow H + C_2H_2^{2+} + e.$$

The $C_2H_2^{2+}$ molecular ion is unstable and will break apart into fragments. The ground state and the first few excited states of $C_2H_2^+$ ions are stable [4, 5] while the higher excited states of $C_2H_2^+$ ions may be unstable and will dissociate into neutrals and ions. Later in this paper we try to estimate the upper limit of those possible contributions.

2. Apparatus and experimental methods

2.1. Apparatus

The experiments were done using THIA's (University of Toledo Heavy Ion Accelerator) atomic collision beam line. The schematic of the experimental apparatus is shown in figure 1. A detailed description of the apparatus will be published elsewhere [10]. Briefly, protons

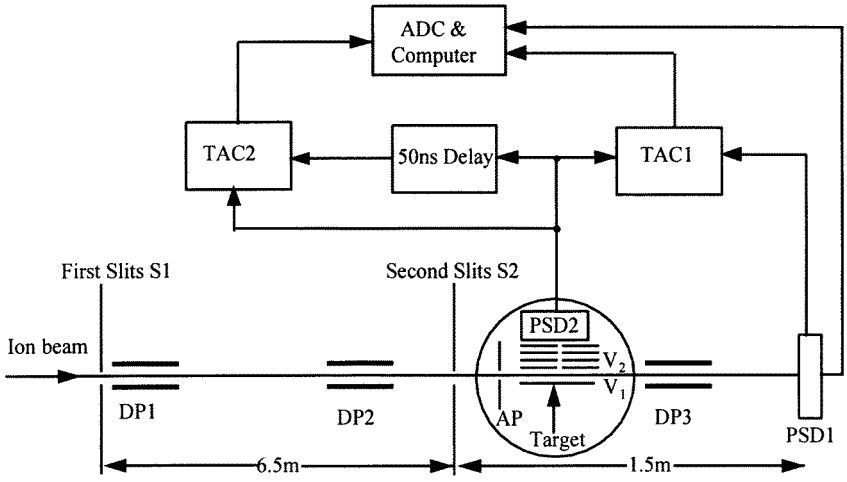

Figure 1. A schematic drawing of the experimental arrangement. DP1: a pair of horizontal plus a pair of vertical deflectors for beam steering. DP2: a combination of three pairs of horizontal, then vertical, and then horizontal deflectors to remove the beam impurities. DP3: a pair of horizontal deflectors that separate the charge states of the projectiles after they collide with the target. AP: a 0.1 mm diameter aperture. V_1 and V_2: extraction voltages to direct the recoil ions towards the detector. PSD1: position sensitive detector for the projectile, and PSD2, for the recoil particles. Target: a gas jet that is directly opposite the recoil detector PSD2.

generated in a conventional ion source are extracted by a potential of 6–20 kV applied to the ion source. The ions are then mass-selected by a bending magnet, accelerated, and directed into the atomic collision beam line. The beam is then collimated by the slits S1 with a slit width in the order of 0.1 mm, where the beam current is reduced from a couple of μA down to the nA range. The ion beam is then deflected by a pair of horizontal and vertical deflection plates (DP1) and then deflected by a combination of three pairs of deflection plates (DP2) configured as horizontal–vertical–horizontal deflections to remove the H^0 and H^- impurity beams that grow as the H^+ beam travels down the beam line and interacts with the background gas. The pure H^+ beam then enters the collision chamber through a 0.1 mm diameter aperture (AP) and collides with target gas molecules that are introduced perpendicularly to the beam through a gas jet. The various charge state (H^+, H^0, and H^-) beams resulting from the collisions with C_2H_2 in the interaction region are separated by a horizontal deflector (DP3) before they impinge on a two-dimensional position sensitive detector (PSD1). Another two-dimensional position-sensitive detector (PSD2) lies 40 mm from the collision centre in the interaction region opposite to the gas jet. The PSD2 is used to detect the recoil products or molecular fragments that are created in the collision region and are extracted by a weak electric field in the interaction region. Timing signals from the PSD1 and the PSD2 are sent to a time-to-amplitude converter (TAC) TAC1 to generate a TOF spectrum to identify the recoil or fragmented products. The timing signal from the recoil detector is also analysed by another TAC (TAC2) to record time intervals between possible two molecular fragments. The recoil timing signal delayed by 50 ns is used to start the TAC2, and the undelayed recoil timing signal is used to stop the TAC2. Using this configuration, time intervals between two fragments with different m/q ratios (mass to charge ratios) can be recorded by the TAC2. The output from TAC1, TAC2, and the position information from the PSD1 are digitally converted, stored and sorted by a computer.

The recoil particles resulting from the electron capture or ionization by the projectile will have small recoil energies. Those recoils which quickly dissociate also will have a kinetic energy of several eV. In order to collect these recoils and fragments, extraction voltages V_1 and V_2 are applied to two plates separated by 2.4 mm with 75 and 50 V DC, respectively, to set up an electric field which accelerates all charged particles in all recoil directions towards the recoil detector PSD2. The extraction voltage ($V_1 - V_2$) of 25 V is chosen for this experimental set-up since a higher voltage would deflect the projectile ions considerably. The front of the PSD2 is biased at -1950 V so that recoil ions with different ratios have a relatively large kinetic energy and thus have the same detection efficiency. The detection efficiency is estimated to be $45\pm4\%$, which is essentially the product of the 55% from the open area ratio of a micro-channel plate and the two 90% transmission grids.

To achieve a good angular resolution, the slit openings for the slit S1 and the slit S2 are set to about 0.1 mm, resulting in an uncertainty of less than 0.002° in angular divergence. The overall angular resolution is about 0.005° due to the 0.15 mm linear resolution from the PSD1 which is about 1.5 m away from the collision centre. Forward scattering angles up to 1.2° can be measured by the PSD1 which has 40 mm diameter micro-channel plates followed by a resistive position encoder.

2.2. Cross sections determination

Cross sections $\sigma_{qq'}$ are determined by the relation $\sigma_{qq'} = Y_{qq'}/(Nnl)$, where $Y_{qq'}$ is the number of counts for scattered projectile charge state q and recoil ions q' (q' can be either C_2H^+, CH^+, or H^+); N is the number of incoming projectiles; n is the C_2H_2 number density in the target interaction region, and l is the length of the interaction region. Since nl was not measured absolutely in this experiment, relative cross sections were acquired. To set these cross sections

on an absolute scale, the following equation is used to relate the quantity $Y_{qq'}$ to the cross section and the target gas pressure:

$$Y_{qq'} = \sigma_{qq'}(nl)N = c\sigma_{qq'}(P_{gas-in} - P_{gas-out})N \tag{1}$$

where c is a normalization constant that can be obtained by using a known cross section for a certain process, and P_{gas-in} and $P_{gas-out}$ are gas pressures in the interaction region with and without the target gas introduced, respectively. In order to limit the collision process to the single collision domain, the net gas pressure ($P_{gas-in} - P_{gas-out}$) is controlled in such a way that it stays the same at 2.0 mTorr for all the runs and the corresponding target thickness nl is estimated to be of the order of 10^{14} particles/cm^2.

2.3. Forward scattering angles

For each process, the forward scattering angles θ were obtained in the following way. First, a linearity check and calibration were carried out by placing a mask of known dimensions in front of the PSD1. Any deviation between the image of the mask obtained by the PSD1 and the real mask was corrected by sorting routines in software. The relative detection efficiency was found to be flat across the detector. Next, the central positions that correspond to projectile charge states H^+ and H^0 were obtained by a peak fitting program, and the central positions served as the references for the scattering angle $\theta = 0$. Azimuthal symmetry was checked to be valid in this experiment and the differential cross section $d\sigma_{qq'}(\theta)/d\Omega$ was obtained by summing all azimuthal angles.

2.4. Normalization

To put our results on an absolute scale, we normalized our relative cross sections to a known differential cross section for $H^+ + He$ under similar experimental conditions. The results for electron capture and single ionization from Shah *et al* [11] were used as the reference cross section for normalization. Their results for 23 keV and 28 keV proton impact on helium were interpolated to give 1.79×10^{-16} cm^2 for electron capture cross section and 2.90×10^{-17} cm^2 for SI cross section at 25 keV. To obtain the normalization constant c in the equation (1), two consecutive runs were carried out for 25 keV proton projectiles colliding with helium target gas and with C_2H_2 target gas at the same pressure with identical software and hardware settings. Impurity signals due to the interaction of the projectile beam with the background residual gas were subtracted from both these runs. Two independent normalization constants, one from the electron capture process with $c_1 = 8.38 \times 10^{17}$ (mTorr^{-1} cm^{-2}), and another from the single ionization process with $c_2 = 8.40 \times 10^{17}$ (mTorr^{-1} cm^{-2}), were averaged to give the final normalization constant $c = 8.39 \times 10^{17}$ (mTorr^{-1} cm^{-2}). This constant was used for normalization of relative cross sections for all projectile energies and all collision processes in order to put the respective relative cross sections on an absolute scale.

3. Results and discussions

Three independent quantities of information were used in the data analysis. The first one is that the projectile position information from the PSD1 indicates the charge states of the scattered projectile beams and is used to separate the ionization channels from the electron capture channels. A typical two-dimensional position information from the PSD1 for 25 keV proton impact on C_2H_2 is shown in figure 2. Events related to ionization or electron capture processes were separated by placing a gate condition on the PSD1 locations corresponding to

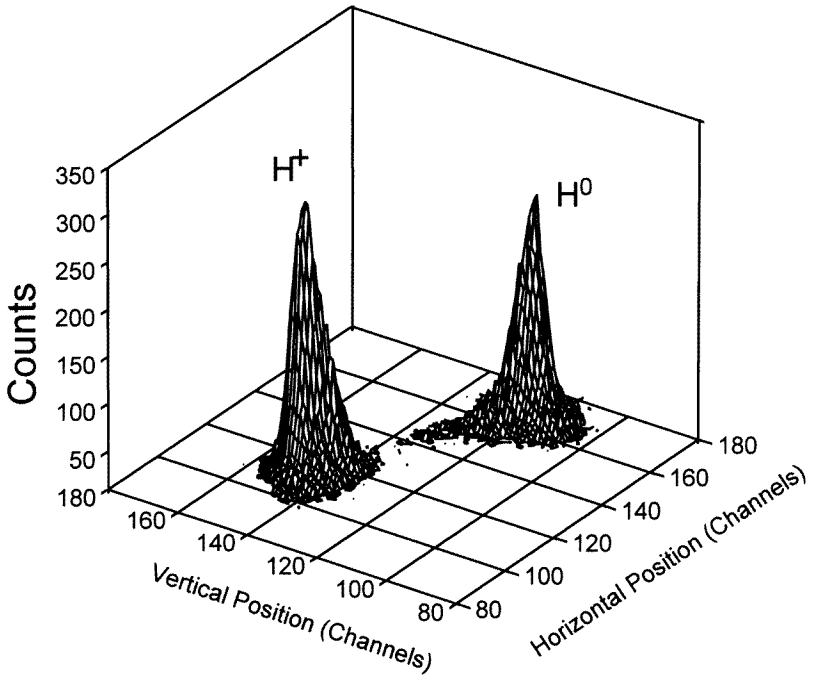

Figure 2. Projectile position information as seen in the PSD1 for 25 keV proton impact on C_2H_2. The display of zero counts has been suppressed for clarity of the graph. The calibration for the projectile detector is such that 104 channels in the graph correspond to 1.0 in physical dimension on the PSD1 anode plane.

H^+ or H^0 when sorting the other data from PSD2. The background signals in the H^+ and H^0 data were measured by turning off the target gas supply and recording those counts at these locations on PSD1. These background counts were subtracted prior to the computation of the cross sections. The other two quantities of information are from timing signals. One is from the TAC1 which records the TOF of the recoils, and the other from the TAC2, which measures the time interval between any possible two consecutive hits on the recoil detector PSD2 by more than one recoil ion generated in the collision. A TOF spectrum from TAC1 and a time interval spectrum from TAC2 for 25 keV proton impact on C_2H_2 is shown in figure 3. Since we are only interested in the cross sections for SI, DI, SC, and TI, the main concern for the TOF is to identify the recoil ions $C_2H_2^+$, and $C_2H_2^{2+}$ which dissociate, and any corrections to these two recoil yields. From the TOF spectrum, figure 3(*a*), three main peaks are identified and the centroids of these three peaks are about 0.44, 1.59, and 2.25 μs respectively for the H^+, CH^+, and $C_2H_2^+$ groups. From the time interval spectrum, figure 3(*b*), three peaks are labelled as peaks (i), (ii), and (iii) for the convenience of discussion. The centroids of the three peaks are at about 0.65, 1.15, and 1.81 μs respectively, which represent time intervals between any two groups from figure 3(*a*).

3.1. $C_2H_2^+$ peak

The recoil ions under the peak labelled in figure 3(*a*) as $C_2H_2^+$ were a combination of real $C_2H_2^+$ ions and possible C_2H^+ and C_2^+ ions which were not resolvable in our set-up due to a short TOF tube. An estimate is necessary to determine the relative contributions to this

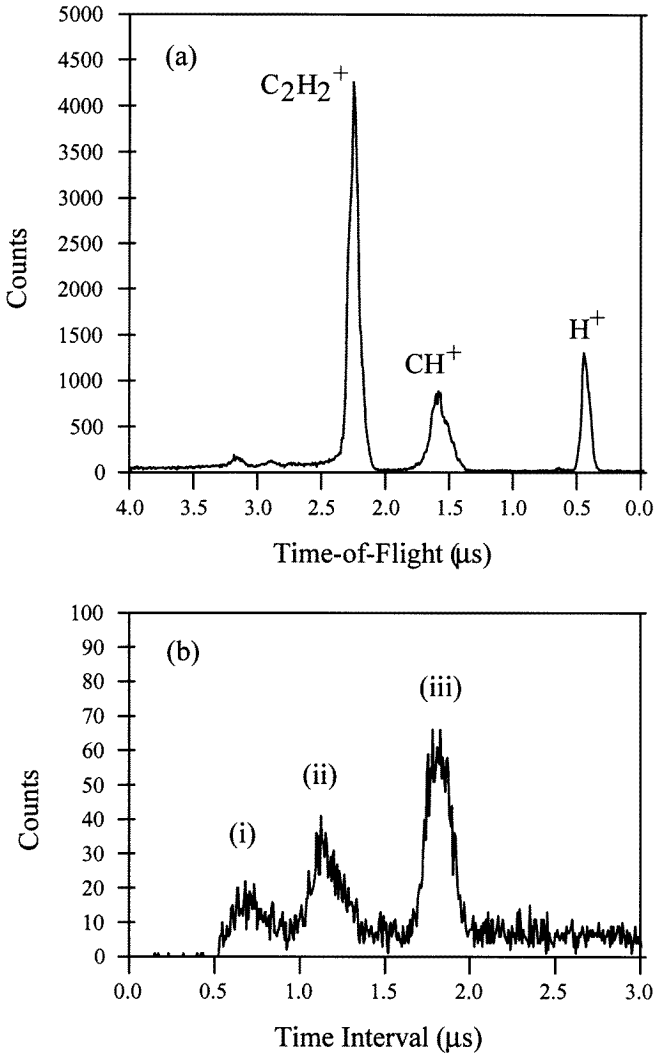

Figure 3. (*a*) TOF spectrum from TAC1 that was generated by a start timing signal from the recoil detector and a stop timing signal from the projectile detector. Note the reversed direction of the time-of-flight scale. (*b*) Time interval spectrum from TAC2 that represents the arrival time difference between any two consecutive hits on the recoil detector. See the text for an explanation of the peaks (i), (ii) and (iii).

peak from the C_2H^+ and C_2^+ channels. The first possible channel is the dissociation of the $(C_2H_2^+)^*$. According to the photoionization data by Hayaishi *et al* [5], the relative efficiency of production of $C_2H_2^+$ and C_2H^+ is about 1 to 0.08, summing over all photon energies. However, this ratio should be much less in ion–molecule collisions since single ionization is considered a one-electron process and ionization plus an excitation is a two-electron process. Another possible source for the C_2H^+ is from the break-up of $C_2H_2^{2+}$ into $C_2H^+ + H^+$. The upper limit of this contribution can be reliably estimated from the peak (iii) in the time interval spectrum, figure 3(*b*). The centroid of the peak (iii) is about 1.8 μs which indicates that contributions to this peak come from the time intervals between one of the recoil ions of the CH_2^+, CH^+, or

C^+, and the H^+ ions. The total counts under the peak (iii) in figure 3(*b*) were about 3.3% (after correction for the detection efficiency for double hit events) of the counts under the peak $C_2H_2^+$ in the figure 3(*a*) TOF spectrum. Finally, the probability for dissociation of $(C_2H_2^+)^*$ into C_2^+ is less than 0.5% [5]. Thus, the main contribution to this peak is from the $C_2H_2^+$.

3.2. CH^+ peak and H^+ peak

These two peaks are discussed together, since they come from the Coulomb break-up of $C_2H_2^{2+}$ ions symmetrically into either $(CH^+ + CH^+)$ or $(C_2 + H^+ + H^+)$. Other break-up channels which produce unequal m/q (mass to charge) ratios were rare, as evidenced in the peaks in figure 3(*b*). The peak (ii) in the spectrum represents the coincidences of H^+ with one of the C^+ or CH^+ ions, and the counts under the peak (ii) was about 2% of the counts from the peaks CH^+ and the H^+ in figure 3(*a*). The peak (i) represents all random coincidences between ions in the (C^+, CH^+, CH_2^+) group and ions in the $(C_2^+, C_2H^+, C_2H_2^+)$ group. The few counts under this peak indicated that random coincidence rate was low and the target thickness was well within the single collision regime.

The relative probability for $C_2H_2^{2+}$ break-up into $(CH^+ + CH^+)$ and $(C_2 + H^+ + H^+)$ then is simply the ratio of the counts under the peak of CH^+ to the counts under the peak H^+ in the TOF spectrum of figure 3(*a*). In order to confirm this claim, the TOF spectrum in figure 3(*a*) was further separated out to a spectrum sorted with a gate condition on the H^+ projectile charge state, which corresponds to ionization processes, and a spectrum sorted with a gate condition on the H^0 projectile charge state, which corresponds to the electron capture process. The ratios

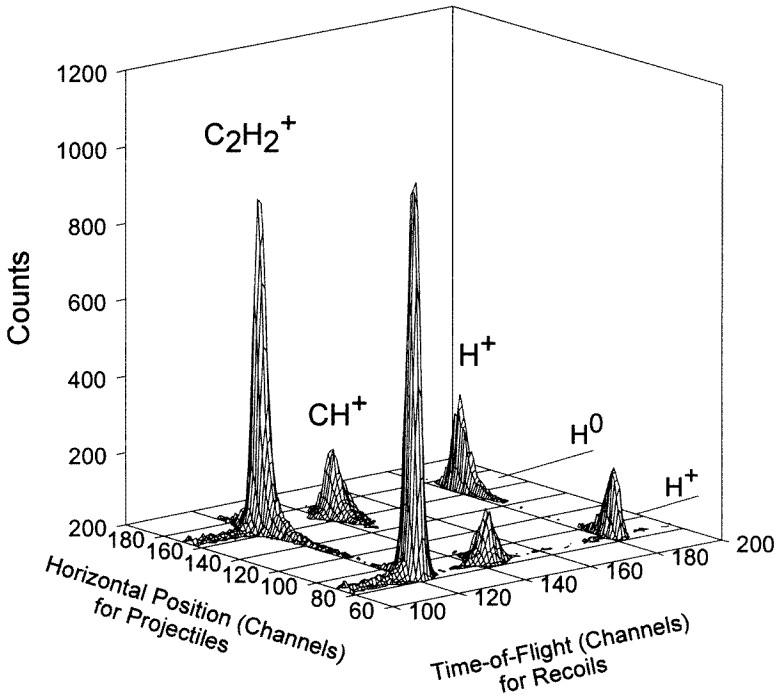

Figure 4. A typical plot of the coincidence between the various scattered projectile charge states and the recoil TOF. The calibration for the TOF is $1\mu s = 31$ channels. The display of zero counts has been suppressed for clarity of the graph.

Table 1. Cross sections (in units of 10^{-17} cm^2) for 6, 12.5, 25, and 50 keV $H^+ + C_2H_2$ collisions. The uncertainties shown in the table are one standard deviation and basically arise from the counting statistics. Systematic uncertainties are discussed in the text.

Energy (keV)	σ_{DI}	σ_{SI}	σ_{TI}	σ_{SC}
6	6.0 ± 0.1	4.4 ± 0.2	4.4 ± 0.1	1.9 ± 0.1
12.5	2.5 ± 0.1	2.5 ± 0.2	12.8 ± 0.3	17.0 ± 0.9
25	8.1 ± 0.2	5.2 ± 0.3	17.3 ± 0.5	9.6 ± 0.6
50	2.8 ± 0.1	5.7 ± 0.2	3.6 ± 0.1	5.4 ± 0.2

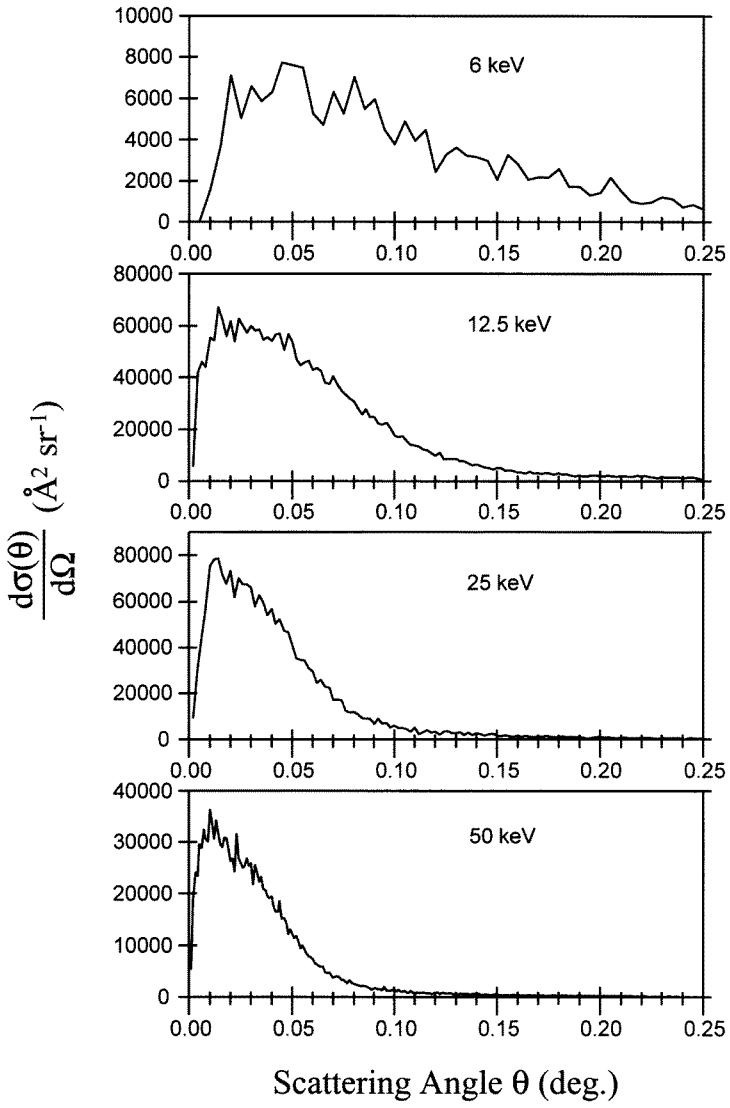

Figure 5. Differential cross sections for SC process of $H^+ + C_2H_2$.

of CH^+ to H^+ counts remain the same for both the DI and the TI processes: 1.42 to 1.0 with a 2% uncertainty due to the counting statistics. This implies that a majority of $C_2H_2^{2+}$ ions break

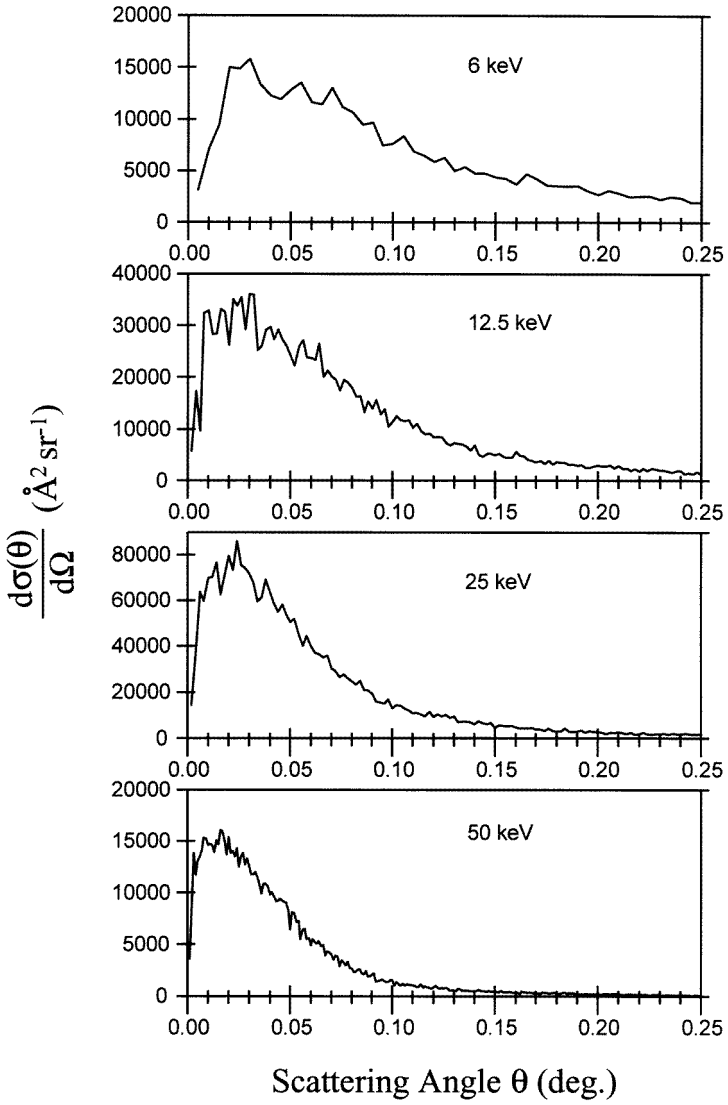

Figure 6. Differential cross sections for TI process of H + C_2H_2.

apart symmetrically. To further prove that there was little contribution to the CH^+ and H^+ timing peaks other than the symmetrical fragmentation channels just discussed, the spectrum for the forward scattering angles sorted with gating conditions on H^+ projectiles and CH^+ recoils was compared with the spectrum sorted with gating conditions on H^+ projectiles and H^+ recoils. The spectra were the same within the counting statistics. This result also applies to the spectra sorted for the H^0 projectile charge state. Therefore, the counts from the CH^+ and H^+ peaks were added together in the determination of the cross sections for double ionization or capture plus ionization.

3.3. Cross sections

To calculate the cross sections, the yields $Y_{qq'}$ for different scattered projectile charge states q were obtained by a coincidence plot of the projectile charge states versus the TOF of the recoils. A typical spectrum of such a plot is shown in figure 4. The contributions from the interaction of the beam with the background residual gas resulting in a change of projectile charge state were corrected before the cross sections were calculated from equation (1). The results are presented in table 1. The errors cited in the table are the compound errors calculated from the counting statistics and the target gas pressure readings only. Other systematic contributions to the error, such as the contributions to the TOF peaks as discussed in the previous sections 3.1 and 3.2, are not included in the uncertainties quoted in table 1.

3.4. Differential cross sections

The differential cross sections for SC and TI processes by the projectile in coincidence with differential recoil species are shown in figures 5 and 6. The general trend is that when the projectile energy increases, the average scattering angle decreases. The average scattering angles associated with H^+ recoils are identical with those associated with CH^+ recoils, which implies that a majority of H^+ and CH^+ ions come from the same parental $C_2H_2^{2+}$ ions. The average scattering angles associated with the $C_2H_2^+$ recoil ions are smaller than those associated with H^+ and CH^+ recoil ions. This is understandable since the generation of $C_2H_2^+$ recoil only requires removal of one electron from the target, which is easier than the removal of two electrons as in the case of production of $C_2H_2^{2+}$ which breaks apart to CH^+ and H^+ recoil ions. Therefore, production of $C_2H_2^+$ ions involves a larger impact parameter than that of CH^+ and H^+ recoils, resulting in a smaller scattering angle for the production of $C_2H_2^+$ recoil ions. The differential cross sections for SI and DI processes show very similar trends and are not presented here.

4. Summary

Collisions of proton and acetylene molecules were studied at laboratory kinetic energies of 6, 12.5, 25 and 50 keV. The total and differential cross sections were measured for SI, DI, SC, and TI processes. A plan is underway to use a longer TOF tube for recoil detection to improve the m/q resolution so that individual recoil charge states can be resolved, and to use a multiple-hit time-to-digital converter to record time intervals between two or more recoils. Together with the position information from the PSD2, molecular orientations of the recoil ions can be reconstructed and the differential cross section observations will be greatly improved since the average over molecular orientation will be avoided, which was the case in this experiment.

Acknowledgments

The authors wish to thank Dr Kamber and Dr Kvale for helpful discussions and comments. This work is partially supported by the University of Toledo Research and Fellowship Programme.

References

[1] Kobayashi K, Tsuchiya M, Oshima T and Yanagawa H 1990 *Origins Life* **20** 99
[2] Gordon K 1997 *PhD Dissertation* The University of Toledo pp 3–4
[3] Kimura M, Li Y, Hirsch H and Buenker R J 1995 *Phys. Rev.* A **52** 1196
[4] Reutt J E, Wang L S, Pollard J E, Trevor D J, Lee Y T and Shirley D A 1986 *J. Chem. Phys.* **84** 3022

[5] Hayaishi T, Iwata S, Sasanuma M, Ishiguro E, Morioka Y, Iida Y and Nakamura M 1982 *J. Phys. B: At. Mol. Phys.* **15** 79
[6] Arusi-Parpar T, Schmid R P, Ganot Y, Bar I and Rosenwaks S 1998 *Chem. Phys. Lett.* **287** 347
[7] Abramson E, Kittrell C, Kinsey J L and Field R W 1982 *J. Chem. Phys.* **76** 2293
[8] Qian J, Green R J and Anderson S L 1998 *J. Chem. Phys.* **108** 7173
[9] Wetmore R W and Schaefer H F 1978 *J. Chem. Phys.* **69** 1648
[10] Cheng S 1999 *AIP Proc. 15th Int. Conf. on the Application of Accelerators in Research and Industry* ed Duggan *et al* (New York: AIP) to be published
[11] Shah M B, McCallion P and Gilbody H B 1989 *J. Phys. B: At. Mol. Opt. Phys.* **22** 3037